ADVANCED MATERIALS INTERFACES
www.advmatinterfaces.de

Hydrazine Sensor Based on Co_3O_4/rGO/Carbon Cloth Electrochemical Electrode

Qian Wang, Meiyan Wu, Shangjun Meng, Xiaoxian Zang, Ziyang Dai, Weili Si, Wei Huang, and Xiaochen Dong**

Porous cobalt oxide (Co_3O_4) nanosheets, vertically aligned on reduced graphene oxide (rGO) modified 3D carbon cloth (CC), are synthesized by using a facile diffusion method at room temperature following a thermal annealing process (named as Co_3O_4/rGO/CC). Employed as freestanding electrochemical electrode, the detection behaviors of the Co_3O_4/rGO/CC toward hydrazine have been systematically investigated. It exhibits a high sensitivity (1306.7 μA mM^{-1} cm^{-2}), good stability, and excellent selectivity. The detection limit for hydrazine can reach to 0.141×10^{-6} M with a linear response range of $5–470 \times 10^{-6}$ M. The outstanding sensing properties of the Co_3O_4/rGO/CC electrode can be attributed to the electrocatalytic activity of porous Co_3O_4 nanosheets, the good conductivity of carbon cloth, and the large surface area of the 3D structure. It presents potential applications in the field of environment protection, food analysis, medicine, and so on.

1. Introduction

Hydrazine (N_2H_4), a difunctional and reactive molecule with powerful reducing capabilities, has received increased attention due to its various applications and concerned carcinogenic effect.[1,2] It has been widely applied in many fields including fuel cells, agricultural, industrial, corrosive inhibitors, pharmacology, military, and aerospace applications.[3,4] However, hydrazine and its derivatives have also been recognized as carcinogenic and hepatotoxic substances, which could cause kidney and liver diseases, even genetic damages or cancer through respiratory system, digestive system, and skin permeation to our body.[2,5,6] Therefore, effective and sensitive detection of hydrazine is practically crucial to environmental and biological analysis. Until now, a lot of methods have been explored for the detection of hydrazine, including chemiluminescence,[7] coulometric,[8] spectrophotometric methods,[9] and electrochemical technique.[10] Because of the straightforward preparation process, sensitivity analysis, and cost-effective operation, electrochemical technique is deemed to the outstanding method for hydrazine detection. However, the electrochemical oxidation of hydrazine at glassy carbon electrode or bare metal is restricted by the high overpotential and sluggish kinetics, which generates a poor detection performance.[11] Although, lots of materials (such as zinc oxide nanonails,[12] ZnO nanorods,[13] polypyrrole nanoplates,[14] etc.) have been used in electrochemical sensors, exploring an efficient and sensitive electrode material is of vital importance.

In the past few decades, carbon-based composites, such as epoxy/carbon fiber,[15] MnO_2/graphene,[16] graphene oxide (GO)/Fe,[17] $MHTiO_2$@C-Au,[18] and $Ni(OH)_2$/3D graphene,[19] have attracted tremendous interests owning to their unique physical and chemical properties. Specially, carbon cloth (CC) composites, consisting of reinforcing carbon fibers and functional nanomaterials, are widely used in microwave absorption,[20] catalysis,[21,22] and supercapacitors,[23,24] due to its excellent mechanical strength, good corrosion resistance, high electrical conductivity, excellent flexibility, and low-cost. However, to our knowledge, the application of carbon cloth in preparing freestanding electrode materials for electrochemical detection devices for hydrazine detection has never been reported.

In this work, porous Co_3O_4 nanosheets, vertically deposited onto the surface of graphene oxide modified carbon cloth, were synthesized through a facile diffusion method at room temperature without the existence of any auxiliary reagents following a thermal annealing process (See **Figure 1**). The GO nanosheets on the surface of CC make the CC present hydrophilic and provide amounts of reactive oxygen functional groups.[25] Furthermore, the GO reduced at high temperature can greatly enhance the conductivity of CC. Compared with the previously reported method of dealing with nitric acid,[26] modified CC with GO was simple and environmental friendliness. More importantly, the constructed Co_3O_4/reduced graphene oxide (rGO)/CC electrode demonstrates high sensitivity, low limit of detection (LOD), and excellent selectivity for hydrazine detection.

2. Results and Discussion

2.1. Structure and Morphology

Figure 2a shows the X-ray diffraction (XRD) patterns of $Co(OH)_2$/GO/CC and Co_3O_4/rGO/CC, respectively. Two diffraction peaks of carbon cloth at $2\theta = 26.23°$ and 44.36°,

Q. Wang, M. Wu, S. Meng, X. Zang, Z. Dai, W. Si, Prof. W. Huang, Prof. X. Dong
Key Laboratory of Flexible Electronics (KLOFE) and Institute of Advanced Materials (IAM)
Jiangsu National Synergetic Innovation Center for Advanced Materials (SICAM)
Nanjing Tech University (NanjingTech)
30 South Puzhu Road, Nanjing 211816, China
E-mail: iamwhuang@njtech.edu.cn; iamxcdong@njtech.edu.cn

DOI: 10.1002/admi.201500691

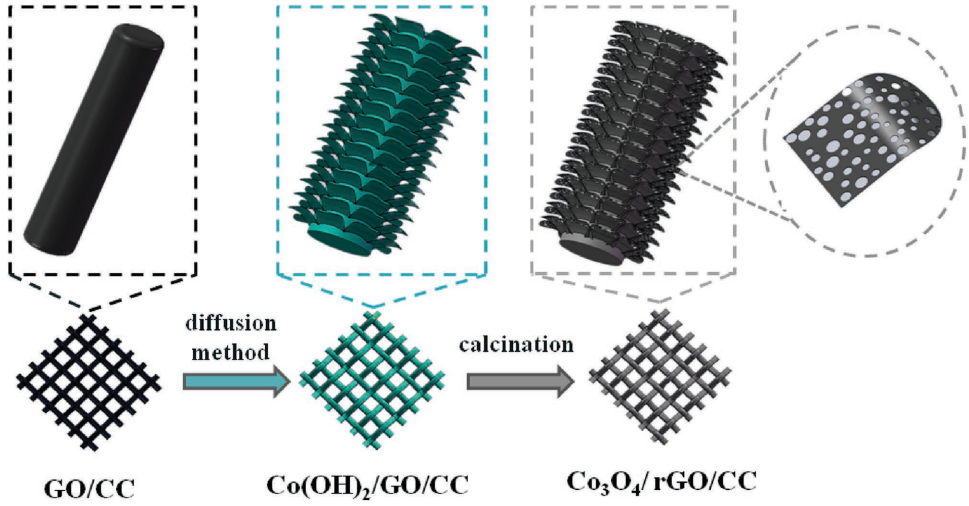

Figure 1. Schematic illustration for the formation of Co_3O_4/rGO/CC.

corresponding to the (002) and (101) reflections of graphite 2H (JCPDS Card no. 75-1621), respectively, can be observed clearly. Meanwhile, at 2θ = 9.502°, 19.162°, 38.033°, and 58.194°, four characteristic diffraction peaks are well indexed to the (001), (002), (102), and (110) phases of $Co(OH)_2$, respectively (JCPDS Card no. 51-1731). In addition, the diffraction peaks at 2θ = 19.000°, 31.271°, 36.845°, 38.546°, 44.808°, 59.353°, and 65.231° are well indexed to the (111), (220), (311), (222), (400), (511), and (440) phases of Co_3O_4, respectively (JCPDS Card no. 43-1003). The XRD spectrum illustrates that the Co_3O_4 grown on the CC has high crystallinity. Figure 2b shows the Raman spectra of CC and CC/rGO/Co_3O_4. The three peaks at about 1360, 1600, and 2750 cm^{-1} correspond to the D, G, and 2D band of CC, respectively. The smaller I_D/I_G ratio after the formation of electrode indicates GO has been reduced to rGO. Especially, the Raman spectrum of CC/rGO/Co_3O_4 presents three distinct peaks at 464, 507, 606, and 675 cm^{-1}, which can be attributed to the vibration mode in cobaltosic oxides phase.[11,27] The Raman spectrum further confirms the formation of Co_3O_4 on the surface of carbon cloth.

Figure 3 shows the scanning electron microscope (SEM) and transmission electron microscope (TEM) images of the carbon cloth, GO/CC, and Co_3O_4/rGO/CC composites. Figure 3a indicates that the carbon cloth is waved by rod-like carbon fibers. The fiber has a smooth surface and the diameter is about 6–8 μm. After modified by graphene oxide, the surface of carbon cloth is relatively roughness and a few wrinkles on the surface of carbon cloth can be observed (Figure 3b). It also confirms that graphene oxide nanosheets have coated onto the surface of carbon cloth uniformly. The SEM image of Co_3O_4/rGO/CC shows that the carbon fibers of carbon cloth are uniformly covered by vertically aligned Co_3O_4 nanosheets (Figure 3c,d). The diameter of the fiber increases to around 10 μm. To further investigate the microstructure of the Co_3O_4, the nanosheets of Co_3O_4 were characterized using TEM, as shown in Figure 3e. It can be observed that the Co_3O_4 nanosheets deposited on the surface of carbon cloth present porous structure, which is useful for the enhancement of surface area. From the N_2 adsorption–desorption isotherms of Co_3O_4 nanosheets (Figure S1, Supporting Information), it can be calculated that the specific surface area is about 72.8 $m^2\ g^{-1}$. In Figure 3f, the high-resolution TEM image exhibits that the Co_3O_4 nanosheets have high crystallinity with the lattice spacing of 0.46 and 0.24 nm, corresponding well to the (111) and (311) plane of Co_3O_4, respectively.

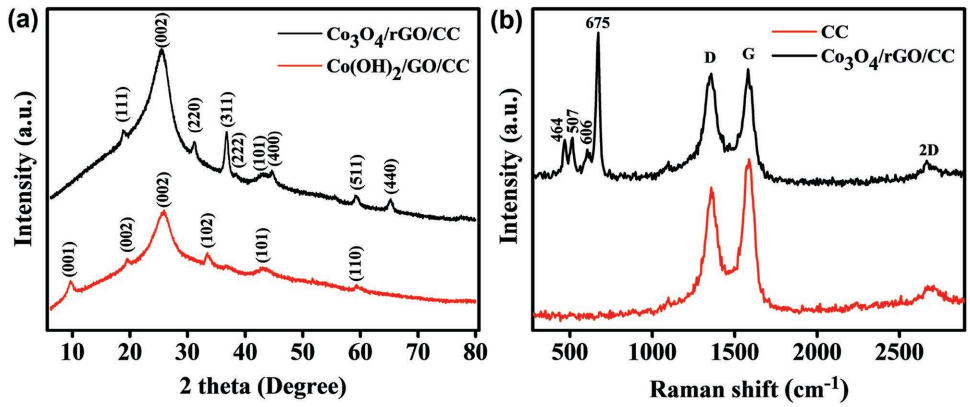

Figure 2. a) XRD patterns of $Co(OH)_2$/GO/CC and Co_3O_4/rGO/CC. b) Raman spectra of CC and Co_3O_4/rGO/CC.

2.2. Electrochemical Behavior of the Co_3O_4/rGO/CC Electrode

The electrochemical performance of Co_3O_4/rGO/CC freestanding electrode was systematically investigated by cyclic voltammogram (CV) and chronoamperometry. **Figure 4**a shows the CV curves of Co_3O_4/rGO/CC and rGO/CC electrodes in 0.1 M sodium hydroxide (NaOH) at a scan rate of 50 mV s^{-1}. No obvious redox peaks were observed in rGO/CC electrode, indicating that the electrochemical activity of the electrode is rather low. On the contrary, a couple of redox peaks can be observed clearly at the potentials of 0.15 and 0.35 V for the Co_3O_4/rGO/CC electrode. These two redox peaks can be attributed well to the reversible electron transfer of Co_3O_4/CoOOH (I/II) and CoOOH/CoO_2 (III/IV),[28] respectively. And these two reversible reactions can be expressed as follows

$$Co_3O_4 + OH^- + H_2O \leftrightarrow 3CoOOH + e^- \quad (1)$$

$$CoOOH + OH^- \leftrightarrow CoO_2 + H_2O + e^- \quad (2)$$

Figure 4b displays the CV curves of Co_3O_4/rGO/CC electrode in 0.1 M NaOH adding different concentrations of hydrazine from 0 to 5×10^{-3} M at a scan rate of 50 mV s^{-1}. With the increasing of hydrazine concentration, the current and potential of anodic peak increase and the cathodic decrease step by step. The oxidation of hydrazine comes from the Co_3O_4 redox intermediates CoO_2. In the anodic sweep, the reduction of CoO_2 and oxidation of hydrazine occurred simultaneously.[11] The reaction of hydrazine and CoO_2 produces CoOOH at ≈0.35 V, which provides amount of CoOOH for further oxidation and makes the anodic current increase. And, the detection mechanism of hydrazine by Co_3O_4/rGO/CC electrode can be illustrated as follows

$$CoOOH + OH^- \rightarrow CoO_2 + H_2O + e^- \quad (3)$$

$$4CoO_2 + N_2H_4 \rightarrow 4CoOOH + N_2 \quad (4)$$

It can be concluded that the determination of hydrazine by Co_3O_4 nanosheets is an indirect process, which is similar with the detection of glucose by Co_3O_4 or other metals in the literature.[11,29,30]

Figure 4c shows the effect of scan rate on hydrazine oxidation at the Co_3O_4/rGO/CC electrode. It can be observed that all the CV curves exhibit two pairs of redox peaks at round 0.15 and 0.35 V, suggesting the redox reaction of Co_3O_4 nanosheets is reversible. With the increasing of scan rate, the anodic peak shows a significantly positive shift, and the cathodic peak shifts negatively simultaneously. Figure 4d demonstrates that anodic and cathodic peak currents of Co_3O_4/rGO/CC electrode scale linearly with the square root of the scan rates, which reveals that Co_3O_4 nanosheets catalytic oxidation of hydrazine is diffusion controlled and the reaction of surface is highly sensitive.[31]

2.3. Amperometric Response of Co_3O_4/rGO/CC to Hydrazine

Employed as freestanding electrochemical electrode for hydrazine detection, the optimal work potential of Co_3O_4/rGO/CC electrode was determined by amperometric response at four

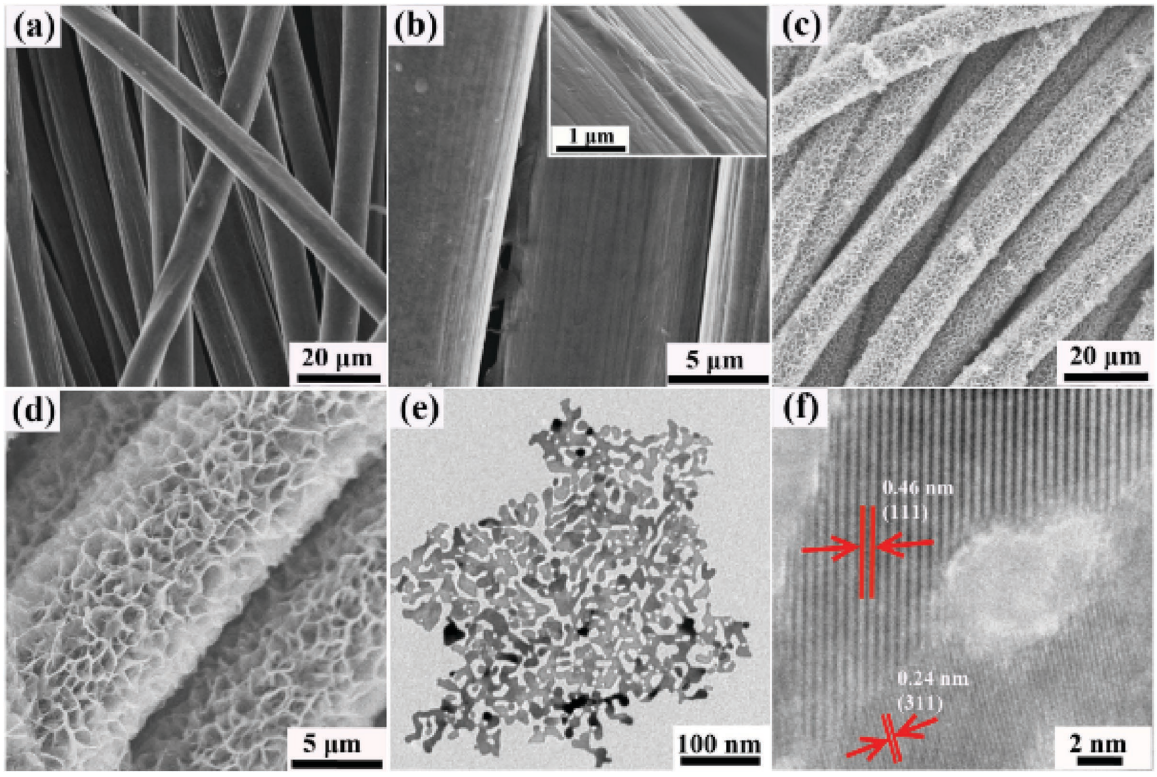

Figure 3. a) SEM image of CC. b) SEM image of CC/GO. Inset shows a magnified image. c,d) Low- and high-magnification SEM images of Co_3O_4/rGO/CC. e,f) Low- and high-resolution TEM images of Co_3O_4 nanosheet.

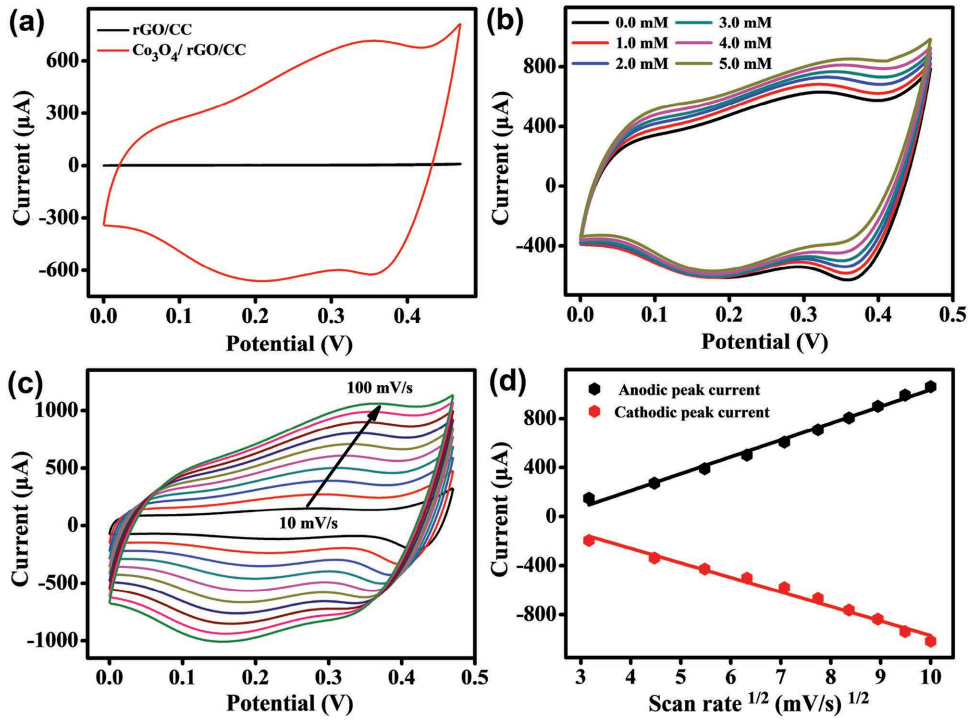

Figure 4. a) CV curves of rGO/CC and Co_3O_4/rGO/CC electrode. b) CV curves of Co_3O_4/rGO/CC electrode containing different concentrations of hydrazine. c) CV curves of Co_3O_4/rGO/CC electrode in 0.5×10^{-3} M hydrazine at diversified scan rates. d) Plots of peak currents at different square root of the scan rate.

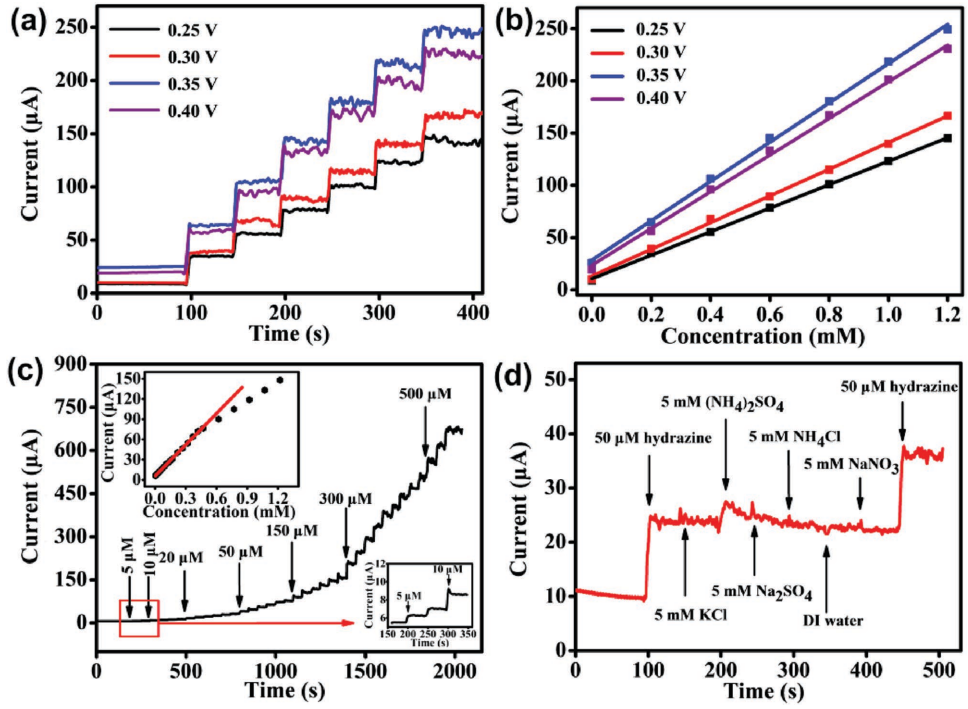

Figure 5. a) Current response of Co_3O_4/rGO/CC electrode to the addition of hydrazine at different potentials. b) Effects of hydrazine concentration on current response at different potentials. c) Typical current response of Co_3O_4/rGO/CC electrode to the consecutive addition of hydrazine in 0.1 M NaOH. Bottom inset is the current response to the addition of 5 and 10×10^{-6} M hydrazine. Top inset is the relationship between response current and hydrazine concentration. d) Amperometric response of Co_3O_4/rGO/CC electrode toward adding hydrazine and various interfering compounds.

Table 1. Hydrazine detection properties of the Co_3O_4/rGO/CC electrode compared with literatures reported previously.

Electrode	Sensitivity [μA mM^{-1} cm^{-2}]	Detection limit [$\times 10^{-6}$ M]	Linear range [$\times 10^{-6}$ M]	ref.
MnO_2/GO	1007	0.16	3.0–1120	[1]
Co_3O_4 NPs	312.7	2.8	20–400	[11]
Hexacyanoferrate/graphite	40	–	100–6000	[33]
Ferrocene/carbon nanotube	358.3	0.6	0.85–700	[34]
CuO hollow spheres	578	1.9	5.0–10 000	[35]
$Mn_7O_{13}{\cdot}5H_2O/\alpha$-$MnO_2$	109.6	2.06	30–2830	[36]
Co_3O_4 NWs	402.8	0.5	20–700	[11]
Co_3O_4/rGO/CC	1306.7	0.141	5.0–470	This work

different potentials with the consecutive addition of 0.2×10^{-3} M hydrazine. In **Figure 5**a, at four different detection potential (0.20, 0.30, 0.35, and 0.4 V), obvious current response can be seen on each addition of hydrazine. While the linear relationship between the hydrazine concentration and response current (Figure 5b) indicates that the sensitivity (calculated from the slope of the calibration curve) of potential at 0.35 V is higher than that of others. So, the detection potential in this experiment is selected at 0.35 V. Figure 5c shows the amperometric response of Co_3O_4/rGO/CC electrode to the successive addition of hydrazine into 0.1 M NaOH solution at a working potential of 0.35 V. Upon adding hydrazine, the steady-state current was obtained in less than 6 s, which indicates that Co_3O_4/rGO/CC electrode possesses rapid and sensitive response characteristics to hydrazine. This phenomenon maybe comes from the fact that rGO/CC has low resistance and large electron transfer rate, which greatly reduces the current response time.[32] The corresponding calibration curve (the top inset in Figure 5c) demonstrates that the Co_3O_4/rGO/CC electrode has a high sensitivity (1306.7 μA mM^{-1} cm^{-2}) for hydrazine detection in the linear concentration range of 5–470 $\times 10^{-6}$ M with a slope of 156.8 μA mM^{-1} and a correlation coefficient of 0.999. The calculated low LOD is 0.141×10^{-6} M (signal/noise = 3). For the comparison, the hydrazine sensing performance of pristine Co_3O_4 coated on glass carbon electrode was also measured. As shown in Figure S3 (Supporting Information), both the sensing sensitivity and stability of pristine Co_3O_4 are not better than that of Co_3O_4/rGO/CC electrode. These results further indicate that Co_3O_4/rGO/CC electrode presents an excellent hydrazine detection performance.

To have a deep understanding of the Co_3O_4/rGO/CC electrode to the hydrazine detection, the comparison with the literature reported typical electrochemical materials is listed in **Table 1**. It can be concluded that the carbon cloth based freestanding Co_3O_4/rGO/CC electrode possesses a higher sensitivity and lower LOD toward hydrazine detection. The superior hydrazine detection performance of the Co_3O_4/rGO/CC electrode can be attributed to the synergistic effects of the porous Co_3O_4 nanosheets and rGO modified carbon cloth. Here, the Co_3O_4 nanosheets provide high catalytic activity and the carbon based 3D network affords high conductivity and large electron transfer rate. Moreover, the vertically grown Co_3O_4 nanosheets on the surface of carbon cloth are in favor of the access of hydrazine to Co_3O_4, which enhances the electrochemical response toward hydrazine oxidation.

Figure 5d presents the selectivity of Co_3O_4/rGO/CC electrode to hydration and other interfering compounds, such as ammonium chloride (NH_4Cl), sodium nitrate ($NaNO_3$), ammonium sulfate ($(NH_4)_2SO_4$), sodium sulfate crystal ($Na_2SO_4{\bullet}10H_2O$), potassium chloride (KCl), and so on. Compared with hydration, there is almost no evident current response when the interfering species are added. Even the concentration of the interfering species is expanded 100-fold than that of hydrazine. These results further indicated that Co_3O_4/rGO/CC electrode exhibits good sensitivity and excellent selectivity for hydrazine detection.

3. Conclusion

In summary, a Co_3O_4/rGO/CC electrode was fabricated using rGO modified carbon cloth as freestanding skeleton. Measurements indicated that the porous Co_3O_4 nanosheets vertically and uniformly aligned onto the surface of the modified carbon cloth. Employed as a freestanding electrochemical electrode, Co_3O_4/rGO/CC electrode presents excellent hydrazine detection performance in terms of response time, sensitivity, selectivity, and linear calibration. Therefore, it will be the more promising materials for fabricating electrochemical electrode for practical hydrazine sensors in the future.

4. Experimental Section

Materials and Reagents: Ethanol, methyl alcohol (MeOH), acetone, and hydrazine hydrate ($H_2NNH_2{\bullet}H_2O$) were commercially available analytical grade reagents and purchased from Shanghai Lingfeng Chemical Reagent Co., Ltd. (Shanghai, China). Cobalt nitrate hexahydrate ($Co(NO_3)_2{\bullet}6H_2O$), 2-methylimidazole, sodium chloride (NaCl), NaOH, NH_4Cl, $NaNO_3$, $(NH_4)_2{\bullet}SO_4$, $Na_2SO_4{\bullet}10H_2O$, and KCl were obtained from Aladdin (USA). GO was synthesized by a modified Hummers method from natural graphite. The CC (W0S1002) purchased from Taiwan CeTech with the thickness of 360 μm and basis weight of 125 g m^{-2}.

Synthesis of Co_3O_4/rGO/CC: First, CC was cleaned with acetone, deionized (DI) water, and ethanol, respectively, by sonification. To enhance the hydrophilic property, the cleaned CC was soaked in GO solution (0.7 mg mL^{-1}) for one week. Then, CC was taken out from GO solution and dried at 60 °C overnight. The porous Co_3O_4 nanosheets, vertically attached onto the GO modified carbon cloth, were synthesized by a facile dispersion method following a thermal annealing process. In a typical experiment, 0.29 g of $Co(NO_3)_2{\bullet}6H_2O$ and 0.16 g of 2-methylimidazole were dissolved in 3 mL MeOH. Then, the modified GO/CC was transferred to the mixed solution and reacted for 24 h at room temperature. After that, the green CC/GO/$Co(OH)_2$ was rinsed with DI water and dried at 60 °C for 12 h. Finally, the dried sample was annealed at 300 °C in air and obtained Co_3O_4/rGO/CC, which could be fabricated into the freestanding electrochemical electrode. Figure 1 shows the schematic illustration for the formation of Co_3O_4/rGO/CC.

Instruments and Electrochemical Measurements: The morphology of the sample was conducted on an SEM (Hitachi S-4800) and

TEM (JEOL JEM-2010). The structure of Co_3O_4/rGO/CC was characterized using an XRD (Bruker D8 Advance) with Cu-Kα radiation (λ = 1.5418 Å). Electrochemical measurements were carried out on a CHI660C electrochemical station (Shanghai China) equipped with a standard three-electrode cell with 0.1 M NaOH solution as the electrolyte. The Co_3O_4/rGO/CC was used as the working electrode (electrochemical active surface area is 0.12 cm^2, the weight percent of Co_3O_4 in Co_3O_4/rGO/CC is about 7.7%). At the same time, Ag/AgCl and platinum wire were used as the reference electrode and counter electrode, respectively.

Supporting Information

Supporting Information is available from the Wiley Online Library or from the author.

Acknowledgements

This work was supported by the Key University Science Research Project of Jiangsu Province (15KJA430006), 973 program (2014CB660808), Jiangsu Provincial Founds for Distinguished Young Scholars (BK20130046), the NNSF of China (61525402, 21275076, and 61328401), Program for New Century Excellent Talents in University (NCET-13-0853), QingLan Project, Synergetic Innovation Center for Organic Electronics and Information Displays, and the Priority Academic Program Development of Jiangsu Higher Education Institutions (PAPD).

Received: October 28, 2015
Revised: December 17, 2015
Published online:

[1] J. Lei, X. Lu, W. Wang, X. Bian, Y. Xue, C. Wang, L. Li, *RSC Adv.* **2012**, *2*, 2541.
[2] B. A. Aigner, U. Darsow, M. Grosber, J. Ring, S. G. Plotz, *Dermatology* **2010**, *221*, 300.
[3] K. Yamada, *J. Power Sources* **2003**, *115*, 236.
[4] N. B. Patel, I. H. Khan, S. D. Rajani, *Eur. J. Med. Chem.* **2010**, *45*, 4293.
[5] C. A. Reilly, S. D. Aust, *Chem. Res. Toxicol.* **1997**, *10*, 328.
[6] S. Tafazoli, M. Mashregi, P. J. O'Brien, *Toxicol. Appl. Pharmacol.* **2008**, *229*, 94.
[7] Z. K. He, X. L. Liu, Q. Y. Luo, H. W. Tang, X. M. Yu, H. Chen, Y. E. Zeng, *Microchem. J.* **1996**, *53*, 356.
[8] T. J. Pastor, V. J. Vajgand, V. V. Antonijevic, *Mikrochim. Acta* **1983**, *3*, 203.
[9] A. Afkhami, A. R. Zarei, *Talanta* **2004**, *62*, 559.
[10] Y. You, Y. Yang, Z. Yang, *J. Solid State Electrochem.* **2012**, *17*, 701.
[11] J. Zhang, W. B. Gao, M. L. Dou, F. Wang, J. J. Liu, Z. L. Li, J. Ji, *Analyst* **2015**, *140*, 1686.
[12] A. Umar, M. M. Rahman, S. H. Kim, Y. B. Hahn, *Chem. Commun.* **2008**, 166.
[13] R. Ahmad, N. Tripathy, D. U. Jung, Y. B. Hahn, *Chem. Commun.* **2014**, *50*, 1890.
[14] J. Ding, K. Zhang, G. Wei, Z. Su, *RSC Adv.* **2015**, *5*, 69745.
[15] F. S. Wang, N. Ding, Z. Q. Liu, Y. Y. Ji, Z. F. Yue, *Compos. Struct.* **2014**, *117*, 222.
[16] X. Feng, Z. Yan, N. Chen, Y. Zhang, Y. Ma, X. Liu, Q. Fan, L. Wang, W. Huang, *J. Mater. Chem. A* **2013**, *1*, 12818.
[17] D. Lin, C. R. Liu, G. J. Cheng, *Acta Mater.* **2014**, *80*, 183.
[18] H. Geng, X. Cao, Y. Zhang, K. Geng, G. Qu, M. Tang, J. Zheng, Y. Yang, H. Gu, *J. Power Sources* **2015**, *294*, 465.
[19] B. Zhan, C. Liu, H. Chen, H. Shi, L. Wang, P. Chen, W. Huang, X. Dong, *Nanoscale* **2014**, *6*, 7424.
[20] J. Zeng, J. Xu, *J. Alloys Compd.* **2010**, *493*, L39.
[21] F. Yang, K. Cheng, G. Wang, D. Cao, *J. Power Sources* **2015**, *290*, 35.
[22] T. Zhang, Y. Zhou, X. Bu, Y. Wang, F. Qiu, *Ceram. Int.* **2015**, *41*, 12504.
[23] S. J. He, W. Chen, *J. Power Sources* **2015**, *294*, 150.
[24] H. Wang, X. Wang, *ACS Appl. Mater. Interfaces* **2013**, *5*, 6255.
[25] D. R. Dreyer, S. Park, C. W. Bielawski, R. S. Ruoff, *Chem. Soc. Rev.* **2010**, *39*, 228.
[26] H.-J. Oh, J.-H. Lee, H.-J. Ahn, Y. Jeong, Y.-J. Kim, C.-S. Chi, *Thin Solid Films* **2006**, *515*, 220.
[27] X. C. Dong, H. Xu, X. W. Wang, Y. X. Huang, M. B. Chan-Park, H. Zhang, L. H. Wang, W. Huang, P. Chen, *ACS Nano* **2012**, *6*, 3206.
[28] Y. Ding, Y. Wang, L. Su, M. Bellagamba, H. Zhang, Y. Lei, *Biosens. Bioelectron.* **2010**, *26*, 542.
[29] C. W. Kung, C. Y. Lin, Y. H. Lai, R. Vittal, K. C. Ho, *Biosens. Bioelectron.* **2011**, *27*, 125.
[30] Q. Yan, Z. Wang, J. Zhang, H. Peng, X. Chen, H. Hou, C. Liu, *Electrochim. Acta* **2012**, *61*, 148.
[31] J. Zhao, J. Liu, S. Tricard, L. Wang, Y. Liang, L. Cao, J. Fang, W. Shen, *Electrochim. Acta* **2015**, *171*, 121.
[32] G. Zhang, S. Hou, H. Zhang, W. Zeng, F. Yan, C. C. Li, H. Duan, *Adv. Mater.* **2015**, *27*, 2400.
[33] R. E. Sabzi, E. Minaie, K. Farhadi, M. M. Golzan, *Turk. J. Chem.* **2010**, *34*, 901.
[34] D. Afzali, H. Karimi-Maleh, M. A. Khalilzadeh, *Environ. Chem. Lett.* **2010**, *9*, 375.
[35] S. B. Khan, M. Faisal, M. M. Rahman, I. A. Abdel-Latif, A. A. Ismail, K. Akhtar, A. Al-Hajry, A. M. Asiri, K. A. Alamry, *New J. Chem.* **2013**, *37*, 1098.
[36] J. Wu, T. Zhou, Q. Wang, A. Umar, *Sens. Actuators, B* **2016**, *224*, 878.